TOWARDS A VIRTUAL PROCESS CHAIN FOR GLASS MAT THERMOPLASTICS (GMT) AS A BASIS FOR DIGITAL PRODUCT DEVELOPMENT

Dominik Dörr
University of Western Ontario (UWO), Faculty of Engineering, Canada
SIMUTENCE GmbH, Germany

Navraj Singh-Heer
University of Western Ontario (UWO), Faculty of Engineering, Canada

Ryan C. R. Gergely
GM Research and Development, General Motors, MI, USA

David Okonski
GM Research and Development, General Motors, MI, USA

Frank Henning
University of Western Ontario (UWO), Faculty of Engineering, Canada
Karlsruhe Institute of Technology (KIT), Institute of Vehicle System Technology (FAST), Germany
Fraunhofer Institute for Chemical Technology (ICT), Department for Polymer Engineering, Germany

Anthony G. Straatman
University of Western Ontario (UWO), Faculty of Engineering, Canada

Andrew Hrymak
University of Western Ontario (UWO), Faculty of Engineering, Canada

Abstract

Chopped fiber materials reveal the potential to be used for complex geometries, offering great potential for functional lightweighting. The material targeted within this study is Tepex flowcore, a long glass fiber reinforced polyamide (PA/GF) glass mat manufactured by Lanxess. Tepex flowcore consists of long glass fibers with random orientation and belongs to the material class of GMT with an engineering polymer, i.e. PA6. Press molding of flowcore can be divided into two different stages, namely material forming and material flow. These stages can include challenges like local wrinkling and incomplete mold filling, respectively. Moreover, manufacturing might be accompanied by process-induced deformations (PID) after solidification and ejection from the mold, the so-called warpage. In this study, a sequential simulation approach including the sub-steps forming, flow, and warpage simulation is presented. Using this approach, the best-suited numerical technique is chosen for each sub-step, while constitutive modeling remains continuous through a unified material modeling approach and the retainment of relevant state variables. The virtual process chain is applied to different geometries with varying complexity and correlated to experimental results for validation.

Introduction

Lightweighting is an important enabler in the modern automotive industry for reducing greenhouse gas emissions and achieving future regulations [1]. For this purpose, continuous fiber reinforced polymers offer great potential due to their excellent weight-specific mechanical properties. However, their capability to be shaped into complex geometries is limited. In contrast, chopped discontinuous fiber reinforced polymers have the potential to be used for more complex geometries, offering a significant opportunity for functional lightweighting [2]. Among

discontinuous fiber reinforced polymers, long fiber reinforced thermoplastics (LFT) have become well established in the automotive industry over the past 20 years as high-performance engineering materials for structural applications [3, 4]. LFT materials can be processed using injection or compression molding. Compression molding enables higher fiber lengths, making this manufacturing technology preferable for structural applications [4]. Among LFT, the main driving force for new thermoplastic composite developments and series applications in the automotive industry was for a long time represented by the group of glass mat thermoplastics (GMT) [3]. Here, it should be noted that several definitions for GMT exist in the literature. Some authors delimit GMT to a polypropylene (PP) matrix [3, 5]. In contrast, Kutz [4] provides a more generalized definition for GMT as being composed of a thermoplastic matrix and glass fibers of 25 mm or more in length. In the past, PP GMT materials have mainly been used and thus also investigated, including textbook knowledge [4, 6, 7, 8]. In contrast, far less is known for GMT with other types of thermoplastic matrices. With an eye toward the developments within Industry 4.0, an established and functional virtual process chain is a powerful tool. The digital twin of the manufacturing process is suitable to support digital product development in the early development phases to optimize the part design concerning the manufacturability and to determine and optimize processing parameters. To the authors' knowledge, virtual process chains particularly suited to GMT materials are investigated sparsely yet [24].

This study proposes a functional virtual process chain for GMT materials, which covers molding and warpage simulation (cf. Figure 1). Molding simulation is split into forming and flow simulation, according to the specific molding behavior of GMT materials. Using this approach, the best-suited numerical technique is chosen for each sub-step, while constitutive modeling remains continuous through a unified material modeling and the retainment of relevant state variables. The considered material is TEPEX® flowcore 102-RGR2400/47%, a GMT with an engineering polymer, i.e. PA6, which is manufactured by Lanxess, Bond Laminates. In the following, the PA6 GMT is classified initially. Subsequently, the modeling approach and related validation for molding and warpage simulation are presented, respectively. Please note that this contribution outlines for brevity only the seminal aspects. For more details, the reader is referred to our studies on the experimental and predictive analysis of GMT molding [9], as well as the characterization for and simulation of GMT molding [10]. The warpage simulation approach and simulation results have not been presented elsewhere yet.

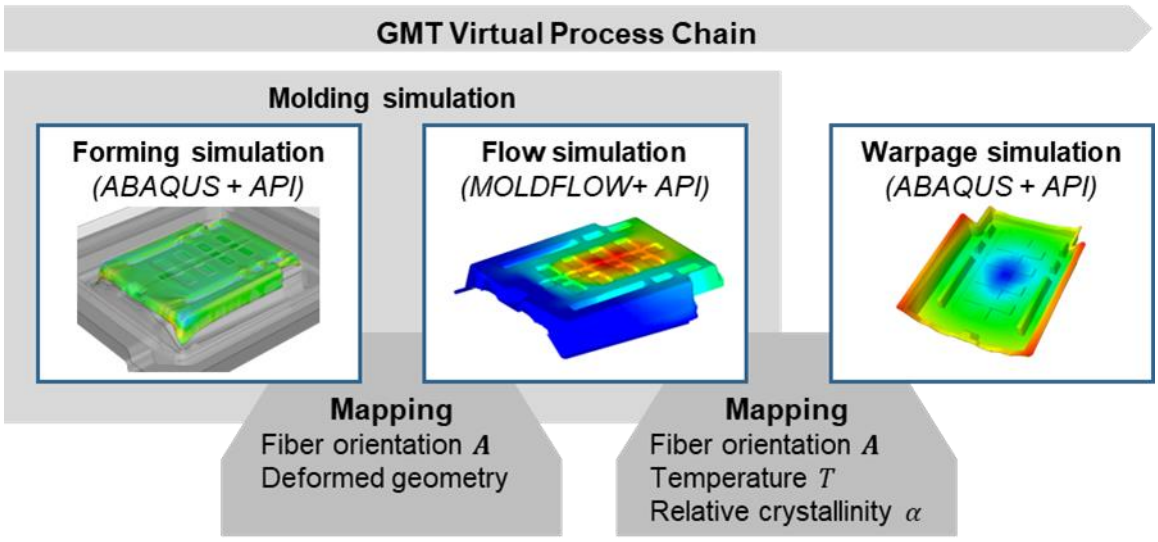

Figure 1: Schematic illustration of the virtual process chain for Glass Mat Thermoplastics (GMT).

Material Classification

The semi-finished product of the investigated PA6 GMT material is manufactured in a continuous process and comes as a sheet in thicknesses ranging from 1 mm to 4 mm. The photographs of a 4 mm sheet in Figures 2 (a) and (b) reveal a macroscopically visible fiber structure with a long fiber length. Moreover, the photo in Figure 2 (a) reveals rolling marks in the 1-direction, which indicate the direction of production of the sheet in the 2-direction.

The exemplary µCT scans in Figures 2 (b) and (c) reveal fibers arranged in bundles with a predominantly in-plane and some out-of-plane alignment from the stacking of the fiber bundles. The quantification of the fiber orientation indicates a moderate scattering with a slightly more pronounced fiber orientation in the direction of production (2-direction).

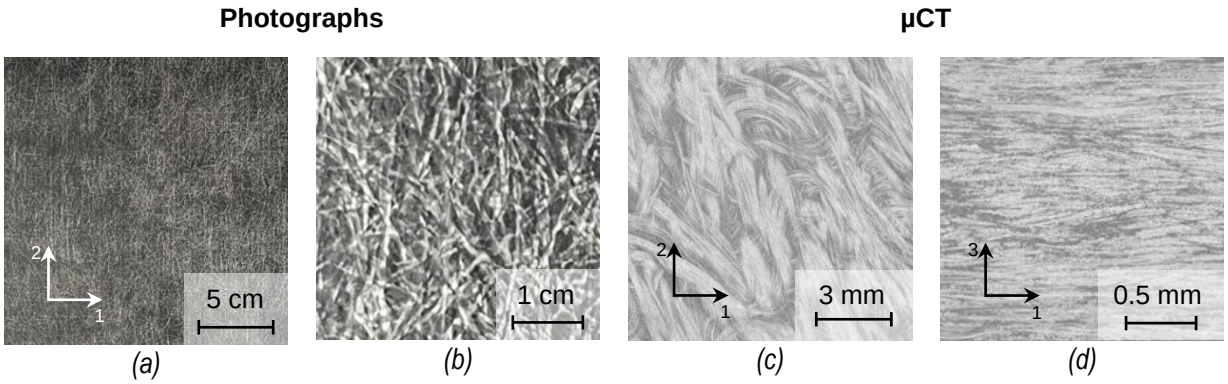

Figure 2: Photos of 4 mm sheet with rolling marks in the 1-direction and direction of production of the semi-finished product in the 2-direction (a, b) and exemplary results from µCT scans for an unmolded 2 mm sheet: In-plane section (c) and through-thickness section (d). [9]

Molding Simulation

A sequential approach is proposed to capture the manufacturing stages of material forming and material flow using ABAQUS® and MOLDFLOW®, respectively, and in combination with related APIs to implement rheological models. This enables a unified material modeling approach, as well as the best-suited numerical technique for each stage. In the following, rheological characterization is outlined initially. Subsequently, the molding simulation approach is applied to different geometries with varying complexity and compared to experimental results for validation.

Rheological Characterization and Modeling

Accurate rheological characterization and modeling are essential for accurate molding analyses. In this study, an in-mold, as well as different rheometer setups for the characterization of viscosity are investigated. Moreover, an anisotropic viscosity model is adopted to capture the rheological behavior.

In-mold characterization. Experimental plaque molding trials are adopted for in-mold (IM) characterization of viscosity on part level. The related shear-edge mold, which is mounted on a Dieffenbacher DCP-U 2500/2200 press, measures in-plane 457 x 457 mm². Stacks of 4 mm flowcore sheets with the dimension 150 x 450 x 16 mm³ are used to induce a 1D material flow. The viscosity is determined as a function of the shear-rate through the gap height and force signal recorded by the press following the approach proposed by Kalaidov et al. [11]. This approach uses the similarity between press and slit rheometry [12] and assumes material in-compressibility as well as a no wall-slip condition.

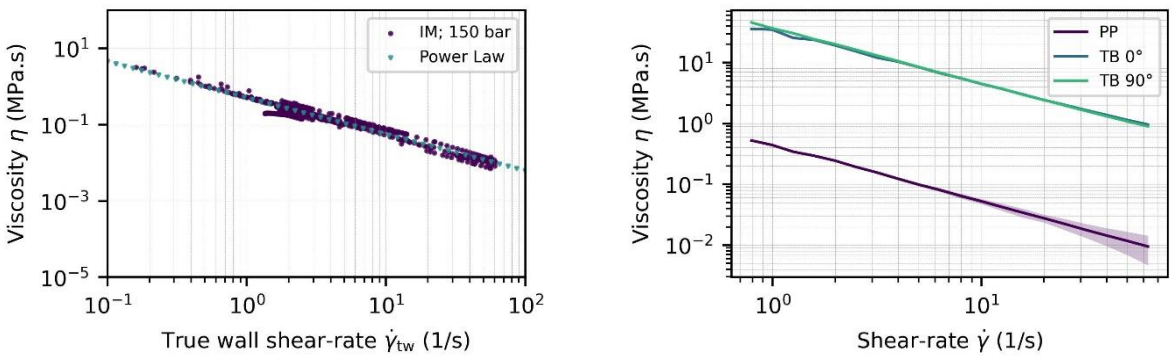

(a) *(b)*

Figure 3: In-mold viscosity (IM) and related Power Law model fit for an exemplary replicate at 150 bar (a) and Comparison of plate-plate (PP) and torsion bar (TB) rheometer results at 280 °C (b). [10]

Figure 3 (a) shows an exemplary result, which reveals that a Power Law model [13] is highly suitable to describe the shear-thinning behavior. A consistency index m of 0.5142 ± 0.0108 MPa.s^n and a flow index n of 0.0760 ± 0.0331 is determined across the specific pressures of 150 and 300 bar and three replicates. Thus, also low scattering is observed between the replicate experiments is observed.

Rheometer characterization. Viscosity is characterized on coupon level using different rheometer setups in oscillatory mode and small strain regime. A plate-plate (PP) setup with a diameter of 25 mm and a gap height of 1 mm is used. In addition, a torsion bar (TB) setup with a width of 13 mm and a testing length of 47 mm is used with a 2 mm sheet.

Figure 3 (b) shows a result for three replicate experiments at 280 °C, which reveals a significantly higher viscosity for the torsion bar compared to the plate-plate tests. It is to be noted that the torsion bar and the plate-plate specimens are sheared in-plane and out-of-plane, respectively, which is in combination with a predominant in-plane fiber orientation an indicator for the anisotropy of viscosity. Therefore, Dinh-Armstrong's [14] equation is used to describe an anisotropic viscosity tensor through

$$\mathbb{V} = 2\bar{\eta}\left[\mathbb{P}_2 + N_\mathrm{p}(\mathbb{A} - 1/3\,\boldsymbol{I} \otimes \boldsymbol{A})\right]. \quad (1)$$

Here, $\bar{\eta}$ is the effective viscosity, $\mathbb{P}_2$ the deviatoric isotropic projector, N_p the dimensionless particle number, $\mathbb{A}$ and $\boldsymbol{A}$ the fourth- and second-order fiber orientation tensors, respectively, and $\boldsymbol{I}$ the second-order identity tensor. The particle number is determined in the scope of this study using Shaqfeh-Fredricksen's equation [15] in combination with experimentally determined fiber volume content and aspect ratio under the assumption of a square fiber packaging. Using the fiber orientation determined through µCT, the remaining parameter in Equation 1 to be determined is the effective viscosity $\bar{\eta}$. Figure 4 (a) shows an exemplary fitting result, where a Power Law model is used to describe viscosity. The results reveal that Dinh-Armstrong's equation is capable to describe the anisotropic viscosity.

Finally, in-mold and plate-plate rheometer characterization is compared. Figure 4 (b) reveals a high degree of agreement between the two different testing methods. Moreover, the plate-plate rheometer characterization results reveal that the shear-thinning dominates the temperature-dependency of viscosity. The Power Law parameterizations extracted above are transferred to a Cross-WLF model [13] to capture the temperature-dependency of viscosity for molding simulation.

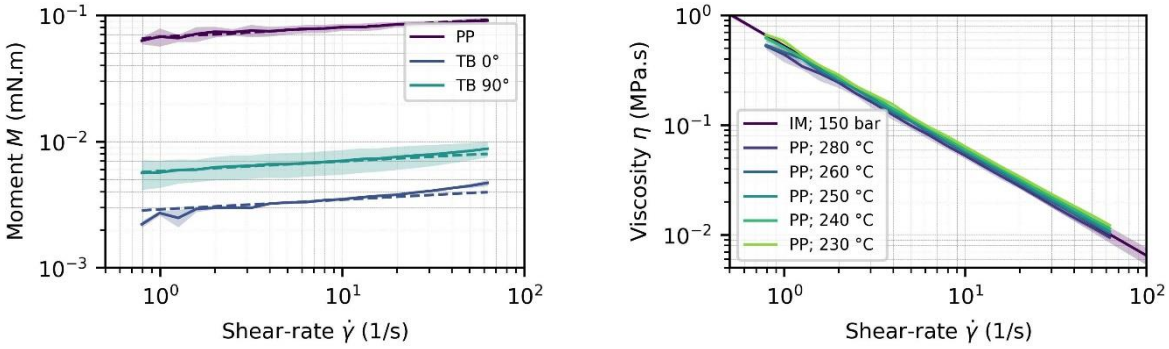

(a) (b)

Figure 4: Comparison of the fitting result for anisotropic viscosity at 280 °C to experimental tests (a) and comparison of viscosity from in-mold (IM) and plate-plate (PP) rheometer testing (b). [10]

Validation of Molding Simulation

Plaque. Molding of plaque does not go along with material forming. Therefore, only material flow is considered for molding simulation. Three different viscosity parameterizations are considered for validation. These are the isotropic in-mold parameterization, the anisotropic rheometer parametrization, and the isotropic rheometer parameterization using the plate-plate rheometer results. Figure 5 shows an exemplary correlation of molding simulation to three experimental replicates for a maximum specific pressure of 150 bar and 300 bar. A high degree of correlation is observed for the rheometer isotropic parameterization for both maximum specific pressures. The in-mold viscosity parameterization yields a similar correlation for 150 bar but predicts a filled plaque for 300 bar. Here, it is to be noted that the plaque is almost filled at 300 bar. A good correlation is achieved with the rheometer anisotropic viscosity parameterization, but the flow lengths are systematically lower compared to the other viscosity parameterizations.

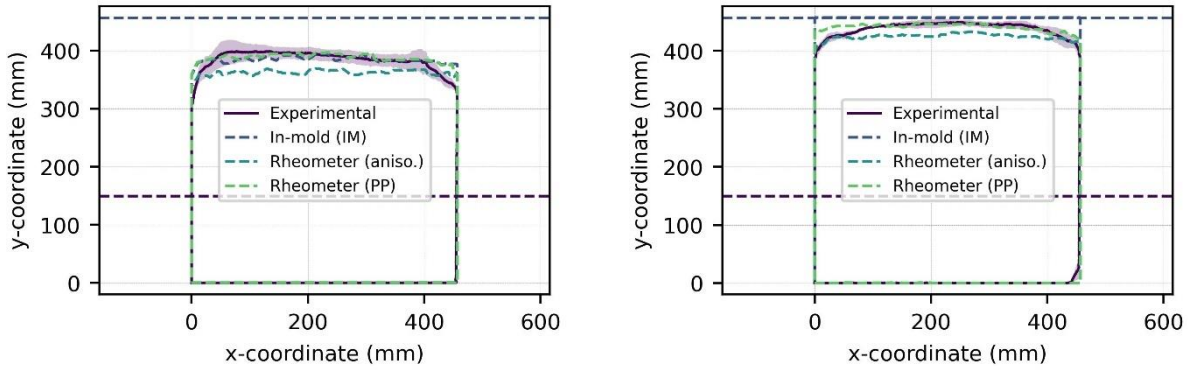

(a) *(b)*

Figure 5: Correlation of plaque molding simulation to three replicate experiments at 150 bar (a) and 300 bar maximum specific molding pressure [10].

Hat section. A hat section geometry with the outer dimensions 957 x 330 x 35 mm³ is used as geometry with intermediate complexity. Here, a forming simulation is conducted and the results are transferred to initialize the material occupation and local fiber orientation for flow simulation. Since molding is dominated by material flow, the PP parameterization is used for simplicity. Figure 6 shows exemplary results for a single sheet with the initial dimensions 950 x 240 x 4 mm³ and a maximum specific pressure of 500 bar. A complete filling of the mold is predicted.

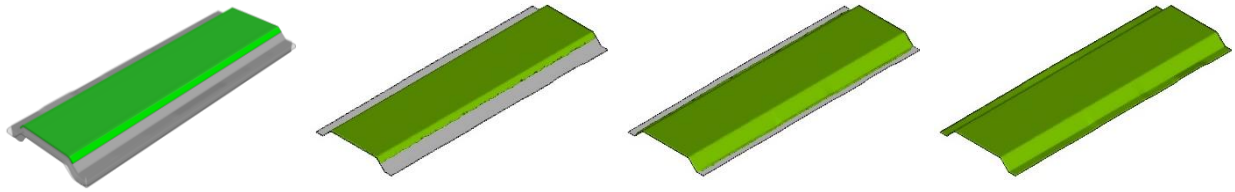

(a) (b) (c) (d)

Figure 6: Hat section molding simulation results: Forming result (a), flow simulation initialization (b), inter-mediate flow result (c), and final result (d).

Experimental tests with varying maximum specific pressures are compared to the related molding simulation in Figure 7 for validation for a single replicate experiment. A filled mold is predicted in agreement with the experimental test for 500 bar. In contrast, incomplete mold filling is predicted for 300 bar and 100 bar maximum specific pressure. This is in agreement with the experimental tests. However, slightly shorter flow lengths as observed in experimental tests are predicted by simulation.

(a) (b) (c)

Figure 7: Comparison of the fitting result for anisotropic viscosity at 280 °C to experimental tests (a) and comparison of viscosity from in-mold (IM) and plate-plate (PP) rheometer testing (b). [10]

Seatback outer. Finally, the so-called seatback outer geometry, which is a complex geometry with deep drawing pockets and beads, is adopted to validate molding simulation also for a complexly shaped geometry. For forming simulation, the anisotropic and the isotropic rheometer parameterization are considered. A sheet tailoring to prevent any material shear-off due to the shear-edge mold is chosen. Figure 8 shows a comparison of an experimental result to the related simulation results. With the anisotropic viscosity parameterization, the horizontal wrinkling between the deep drawing pockets, the vertical wrinkling below the deep drawing pockets, as well as the vertical material accumulation between the deep drawing pockets are in agreement with the experimental test, although especially the horizontal wrinkling is predict-ed less pronounced. In contrast, no wrinkling due to forming of the deep drawing pockets is predicted through the isotropic viscosity parameterization.

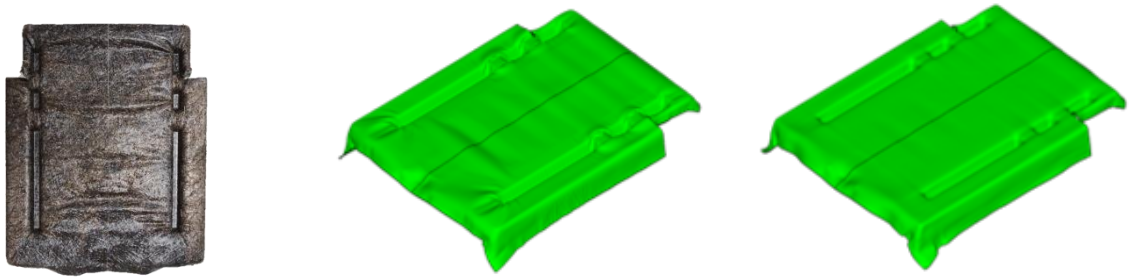

(a) (b) (c)

Figure 8: Seatback outer forming simulation validation: Experimental result (a), anisotropic viscosity (b), and isotropic viscosity (c) [10]

Another sheet tailoring is considered for validation of flow simulation. This tailoring maximizes the material occupation before the onset of material flow but results in material shear-off due to the shear-edge of the mold. Figure 9 (a) shows the MOLDFLOW model setup including the part mesh and the mesh of the initial charge, which has been transferred from the forming simulation in ABAQUS. Incomplete mold filling is observed in four replicate experiments at 300 bar maximum specific pressure. Figure 9 (b) shows an exemplary experimental replicate and Figure 9 (c) the related flow simulation result. Flow simulation predicts incompletely filled part areas in agreement with the experimental tests. A symmetric result is obtained in simulation, whereas a slight asymmetry is observed in the experimental test.

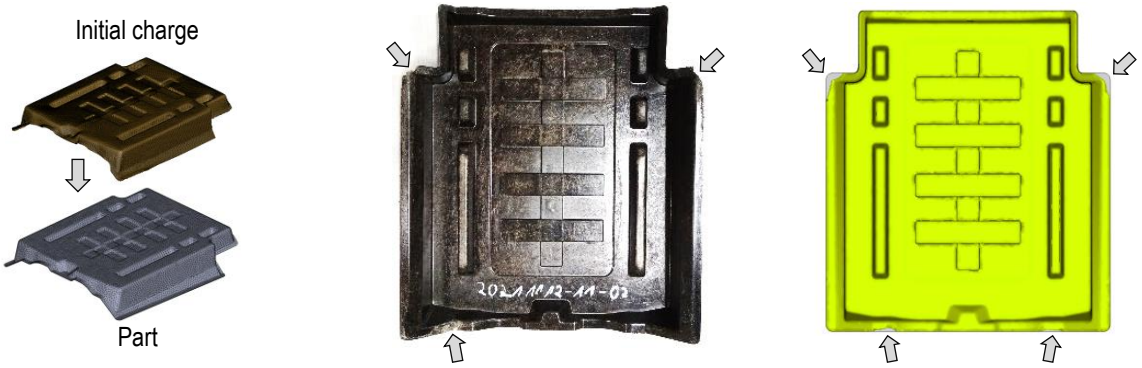

Figure 9: Seatback outer flow simulation validation: Initial charge (top) and part mesh (bottom) in MOLDFLOW (a), exemplary experimental result (b), and flow simulation result (c). [10]

Warpage Simulation

Warpage simulation is based on thermokinetical-thermomechanical modeling of solidification and cooling after the mold is filled. Results from molding simulation for fiber orientation, temperature, and relative crystallinity are considered (cf. Figure 1). Here, thermokinetics predicts the solidification of the polymer melt due to crystallization and thermomechanics predicts the evolution of residual strains and resulting residual stresses and warpage.

Thermokinetical Characterization and Modeling

Differential Scanning Calorimetry (DSC). Thermokinetics is characterized by using two different DSC devices. First, standard DSC is conducted using a DSC Q2000 from TA Instruments. Melting is analyzed using a heating rate of 10 °C/min. Moreover, crystallization is analyzed for low cooling rates (5 C/min and 10° C/min). Second, flash DSC is conducted using a Mettler-Toledo Flash DSC 1 with a Huber intercooler TC100. Here, crystallization kinetics is analyzed for high cooling rates (300 – 1200 °C/min). A linear baseline is used to extract the crystallization enthalpy h_c for crystallization kinetics analysis. The total crystallization enthalpy Δh_c is obtained through time integration over the whole crystallization peak. Based on this, the temporal evolution of the degree of conversion α is obtained through

$$\alpha(t) = \frac{1}{\Delta h_c} h_c(t). \tag{2}$$

It should be noted that in contrast to standard DSC, flash DSC does not enable the measurement of the specific heat flow. Therefore, the relative crystallinity $\boldsymbol{\alpha} \in [\mathbf{0}, \mathbf{1}]$ is adopted for the degree of conversion rather than the absolute crystallinity. The exemplary result from standard DSC in Figure 10 (a) reveals endothermic melting and exothermic crystallization. A melting temperature

of 217.61 ± 0.24 °C is determined from five replicate experiments. The results for the temporal evolution of the degree of conversion as a function of the cooling rate are presented in Figure 10 (b) (solid lines). The onset of crystallization is observed just below 200 °C for the lowest cooling rate, which is pushed towards lower temperatures for higher cooling rates.

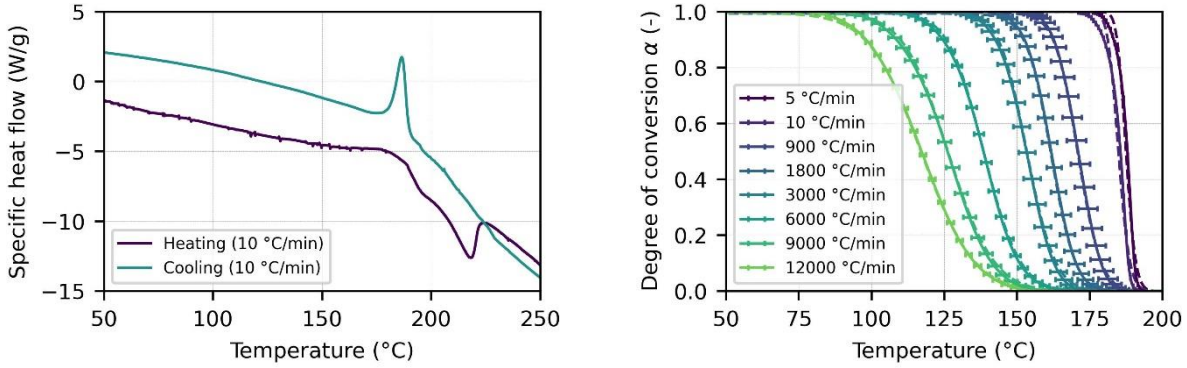

(a) *(b)*

Figure 10: Specific heat flow from standard DSC analysis for heating and cooling at 10 °C/min (a) and degree of conversion determined as a function of the cooling rate from standard DSC (5 °C/min and 10 °C/min) and flash DSC (300 °C/min to 12000 °C/min) (solid lines) and kinetics modeling (dashed lines) (b). [9]

Crystallization kinetics. Crystallization kinetics is modeled using Nakamura's equation [16], which is given in differential form by [17]

$$\dot{\alpha}(t) = nK(T)\big(1-\alpha(t)\big)\ln\left[-(1-\alpha(t)\right]^{\frac{n-1}{n}}. \tag{3}$$

Here, n is the Avrami index and K is the crystallization rate constant. Our previous study [18] has shown that the usually adopted Hoffmann Lauritzen approach [19] to describe the crystallization rate constant K fails to describe crystallization kinetics over a wide range of cooling rates. Therefore, Ziabicki's empirical approach [20] is adopted:

$$K(T) = K_{\max}\exp\left(-\frac{4\ln(2)\,(T-T_{\max})^2}{D^2}\right). \tag{4}$$

where $\boldsymbol{K_{\max}}$, $\boldsymbol{T_{\max}}$, and $\boldsymbol{D}$ are a set of material parameters defined for a specific cooling rate. Figure 10 (b) shows the fitting result, which reveals that Nakamura-Ziabicki's approach is highly suitable to capture crystallization kinetics over a wide range of cooling rates.

Thermomechanical characterization and modeling

Dynamic Mechanical Analysis (DMA). Time- and temperature-dependent mechanical behavior is characterized using a DMA 450+ device from Metravib. The tensile specimens measure 32 x 10 x 2 mm³ and are loaded strain-controlled with an amplitude of 0.05 %. Amplitude sweeps have proven that this amplitude is in the small strain regime. The tested temperatures range from 30.0 to 210.0 °C with an interval of 10 °C and refinement to 5 °C around the glass transition temperature T_g. 9 log-spaced frequencies ranging from 1.0 to 10.0 Hz are tested for each temperature. Figure 11 (a) shows the results of the DMA tests. A decreasing storage modulus towards higher temperatures and a peak in the loss modulus around T_g is observed.

pVT analysis. Pressure-Volume-Temperature characterization is conducted using a GOTECH PVT6000 (piston type) device following ISO 17744, where the material is cooled at 5 °C/min under isobaric conditions at 300, 600, 900, and 1200 bar. A 2-domain Tait model is fitted

upon the characterization data, which is shown in Figure 11 (b). This model parameterization is used on the one hand for the molding simulation described in the previous section. On the other hand, the coefficient of linear thermal expansion (CLTE) in the solid material state, as well as the shrinkage coefficient due to crystallization are extracted at 1.0 bar.

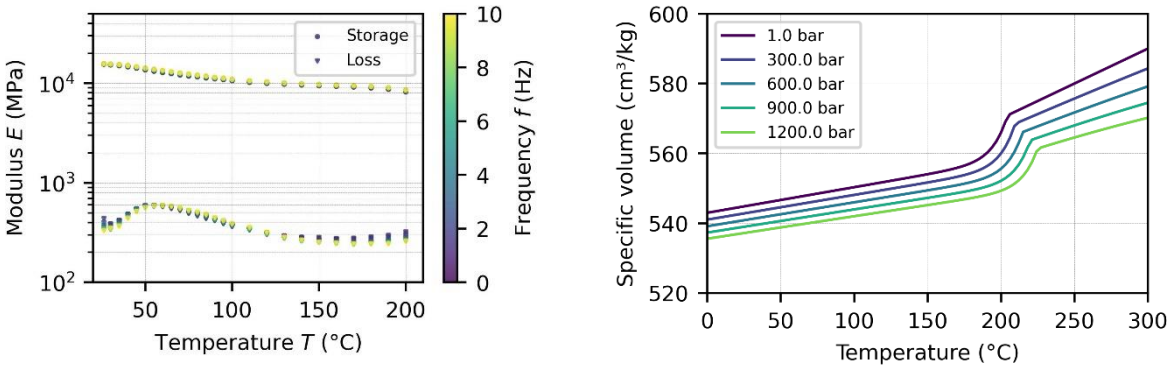

(a) *(b)*

Figure 11: Result from Dynamic Mechanical Analysis (DMA) (a) and 2-domain Tait parameterization (b).

Thermomechanical modeling. The viscoelastic nature of the solidified material needs to be considered for warpage simulation since a significant portion of cooling happens above T_g. In the scope of this study, a path-dependent approach originally developed for thermoset materials [21] is adopted for computational efficiency. This approach is based on a standard linear solid, also known as the Zener model, in Maxwell representation, which consists of a spring element connected in parallel with a Maxwell element. Please note that mold temperature is usually chosen well above the glass transition temperature T_g, which implies short relaxation times after solidification. Thus, the contribution of viscoelasticity is small and elastic rubbery material behavior is to be expected. After part ejection and during further cooling, relaxation times increase, especially as soon as T_g, is undercut. Consequently, viscoelastic properties increasingly participate in stress development and the material exhibits glassy behavior. Assuming a fast switch between rubbery and glassy state, the binary state variable γ is defined:

$$\gamma(T) = \begin{cases} 0, & T \geq T_g - \Delta T_{vitr} \text{ (rubbery)} \\ 1, & T < T_g - \Delta T_{vitr} \text{ (glassy)} \end{cases}. \tag{5}$$

Here, ΔT_{vitr} is the difference in T_g and T where the material vitrifies. Note that the binary state variable γ replaces the damper element in the Maxwell element of the Zener model. Based on this, the total stress ($\boldsymbol{\sigma} = \boldsymbol{\sigma}^{el} + \boldsymbol{\sigma}^{ve}$) is computed through

$$\boldsymbol{\sigma}^{el}(t_n) = \boldsymbol{\sigma}^{el}(t_{n-1}) + \alpha \mathbb{C}_\infty : \Delta\boldsymbol{\varepsilon}, \tag{6}$$

$$\boldsymbol{\sigma}^{ve}(t_n) = \begin{cases} \mathbf{0}, & \gamma = 0 \\ \boldsymbol{\sigma}^{ve}(t_{n-1}) + \alpha \Delta\mathbb{C} : \Delta\boldsymbol{\varepsilon}, & \gamma = 1 \end{cases},$$

where $\mathbb{C}_\infty$ is the rubbery elastic modulus, $\Delta\mathbb{C}$ the difference in rubbery and glassy modulus, and $\Delta\boldsymbol{\varepsilon} = \Delta\boldsymbol{\varepsilon}_{ext} + \Delta\boldsymbol{\varepsilon}_{th} + \Delta\boldsymbol{\varepsilon}_{sh}$ the sum of strain increments of external strain, thermal strain due to linear thermal expansion, and shrinkage strain due to crystallization.

Material homogenization. Molding significantly influences the local fiber orientation through material forming and material flow. The local fiber orientation is predicted and retained along the proposed virtual process chain (cf. Figure 1) through the second-order orientation tensor $\boldsymbol{A}$. This information is adopted for material homogenization to predict the effective local material properties. In the scope of this study, Tandon-Weng's [22], Rosen-Hashin's [23], and Clayton's

[24] approaches are used to homogenize mechanical stiffness, the coefficient of linear thermal expansion as well as the shrinkage coefficient, and the thermal conductivity, respectively. The remaining quantities of heat capacity and material density are independent of the local fiber orientation. Therefore, the properties of the composite are applied directly.

Validation of Warpage Simulation

Finally, warpage simulation is validated through a correlation of the predicted deformed shape to surface scans of a molded part. Surface scans are created using a FARO 3D laser scanner. The resulting point cloud is triangularized using the software PolyWorks. Both the simulation result as well as the experimental surface scan are imported into the software GOM Inspect to align the geometries to the nominal geometry, as well as to compute the local deviation Δu of the actual geometry to the nominal geometry for validation.

Hat section geometry. Figure 12 (a) shows the experimental result for the local deviation of a molded part to the nominal geometry. A significant deviation is observed in the nominal geometry. Moreover, a concave curvature along the length direction and a convex curvature at the edges in the transversal direction are observed. In contrast, a convex curvature is observed for the simulation result. The deviation between the experimental and simulation results is likely to originate from the differential core and cavity temperature in the molding trials, which is observed for injection molding [25], but which is not considered yet in molding simulation.

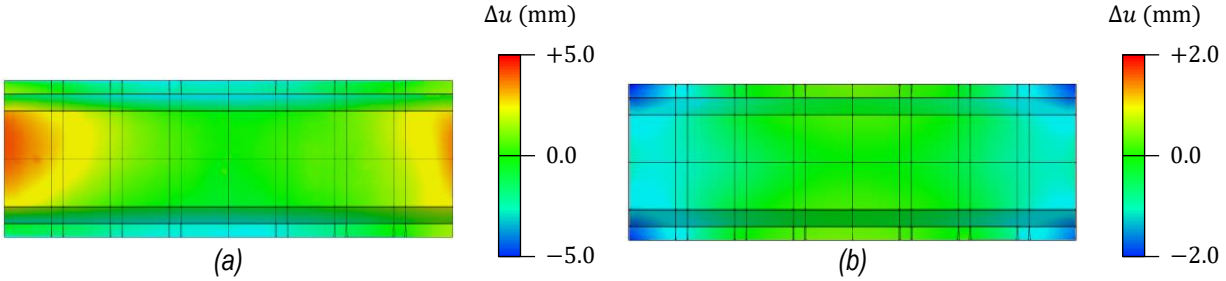

Figure 12: Deviation from actual to nominal geometry for the hat section geometry: Exemplary experimental result (a) and warpage simulation (b)

Seatback outer geometry. Figure 13 (a) shows the experimental result for the local deviation of a molded part to the nominal geometry. The largest deviation is observed at the part flanges. Moreover, some deviation is observed at the bottom area and around the deep drawing pockets. The simulation result is in qualitative agreement. However, the magnitude of warpage observed in in simulation is smaller compared to the experimental test.

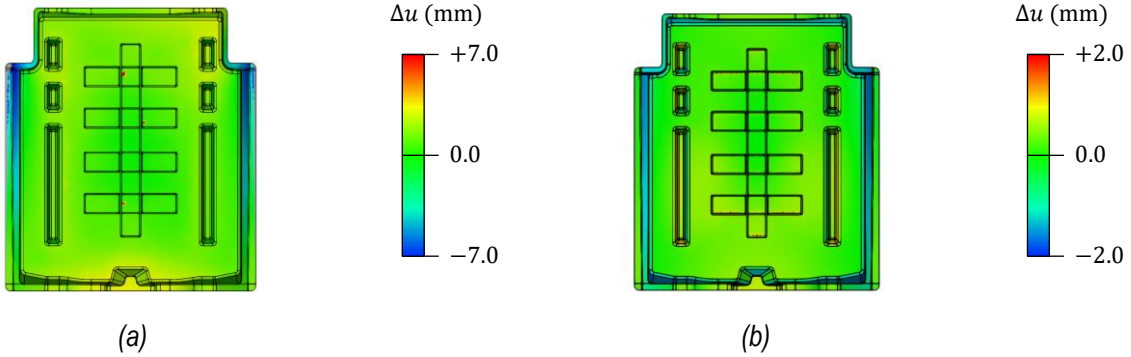

Figure 13: Deviation from actual to nominal geometry for the seatback outer geometry: Exemplary experimental result (a) and warpage simulation (b)

Summary and Conclusion

A virtual process chain for GMT materials, which covers molding and warpage simulation, is proposed. Relevant state variables, including the local fiber, temperature, and relative crystallinity are predicted and retained. Based on this, the virtual design and optimization in the scope of digital product development can be supported through a digital twin of the manufacturing process.

The proposed molding simulation approach splits into the sequential stages of material forming and material flow, according to the specific molding behavior of GMT materials. Based ont this, the best-suited numerical technique is used for each step. Initially, an in-mold characterization approach using solely the data recorded by the press from plaque molding trials is adopted. The resulting viscosity data shows a high correlation to viscosity characterization using a plate-plate rheometer. Therefore, the approach is expected to be highly valuable when press data from plaque molding is already existing or if rheometer tests are not possible. Moreover, the rheological behavior is characterized using different rheometer setups, revealing a strong anisotropy of viscosity, due to the predominant in-plane fiber orientation of the semi-finished product. Adopting Dinh-Armstrong's equation reveals that the observed anisotropy can be captured for molding simulation.

The rheological models are applied to molding simulation for three different geometries. High prediction accuracy is observed for the predicted flow length for a plaque geometry. Here, comparable results are obtained for the anisotropic as well as the isotropic viscosity parameterizations. Besides this, a hat section geometry shows a good correlation for the predicted flow lengths using the parameterization from plate-plate rheometer testing. However, flow lengths are slightly too short. Finally, molding simulation is validated for a complexly shaped geometry. It is observed in the correlation of forming simulation to a partly formed part that the wrinkling behavior observed in experimental tests is predicted solely by the anisotropic viscosity. In contrast, no wrinkling behavior is predicted by the isotropic viscosity. Forming is expected to happen predominantly through in-plane deformation (elongation and bending). The anisotropy of viscosity induces a significant increase in in-plane viscosity, which explains the observed difference. Finally, flow simulation is validated for the complexly shaped geometry, where the unfilled areas predicted by simulation are in high agreement with the experimental result. In summary, anisotropic viscosity modeling enables unified material modeling for forming and flow analyses, whereas an isotropic viscosity is sufficient for flow analyses.

The proposed warpage simulation approach predicts part solidification and cooling in a thermokinetical-thermomechanical analysis, under consideration of local fiber orientation, temperature, and relative crystallinity predicted by molding simulation. Thermokinetics is successfully parameterized upon standard and flash DSC. The viscoelastic material behavior is parameterized using DMA. The coefficient of linear thermal elongation, as well as the shrinkage coefficient, are parameterized using pVT data, which has proven to be more robust and efficient compared to TMA testing. The proposed approach is applied for validation to the hat section and seatback out geometries. A deviating warpage pattern is predicted for the hat section geometry. This is expected to originate from the differential molding temperature not considered yet in the simulation. In contrast, a similar warpage pattern as observed for the experimental test is predicted for the seatback outer geometry. However, the magnitude of the warpage is larger in the experimental test. A feasible origin is residual stresses in molding simulation, which are not transferred yet to warpage simulation (cf. Figure 1). Both differential mold temperatures, as well as the transferring residual stresses, will be part of future research.

Acknowledgments

The authors acknowledge the funding support of General Motors of Canada, Natural Sciences and Engineering Research Council of Canada (Grant CRDPJ 518279-17), and the Ontario Centers of Excellence (Grant VIP2 28722).

The authors greatly appreciate the flash DSC work completed by Xiaoshi Zhang at Penn State Behrend. Moreover, the authors gratefully appreciate the carefully carried out fiber orientation analysis by Trevor Donald Sabiston (University of Waterloo), as well as the professional support on the shop floor by Rob Cosh, Steve Jones, and Keith Ruck (Fraunhofer Innovation Platform @ Western).

Bibliography

1. F. Henning et al., Fast processing and continuous simulation of automotive structural composite components, Composites Science and Technology 171 (2019) 261–279.
2. J. Görthofer et al., Virtual process chain of sheet molding compound: Development, validation and perspectives, Composites Part B: Engineering 169 (2019) 133–147.
3. M. Schemme, LFT – development status and perspectives, Plastics, Additives and Compounding 10 (2008) 38–43.
4. M. Kutz (Ed.), Applied plastics engineering handbook: Processing, materials, and applications, second edition, Elsevier, 2017.
5. D. Burn, Long discontinuous carbon fibre/polypropylene composites for high volume automotive applications, Doctoral thesis, University of Nottingham, 2016.
6. B. A. Davis et al., Compression molding, Hanser, Munich, 2003.
7. D. A. Grove, Composite processes, in Handbook of Plastic Processes, John Wiley & Sons, Inc, Hoboken, NJ, USA, 2005.
8. T. A. Osswald, Polymer processing fundamentals, SPE books, Hanser and Hanser/Gardner, Munich and Cincinnati, 1998.
9. D. Dörr et al., Experimental and predictive analysis of the molding behavior of a PA6 Glass Mat Thermoplastic (GMT), Journal of Composite: Part B, 2022. (submitted)
10. D. Dörr et al., Rheological Characterization and Macroscopic Modeling and Simulation of the Molding Process of a PA6 Glass Mat Thermoplastic (GMT), Journal of Composites: Part A, 2022 (submitted)
11. M. Kalaidov et al., Viscosity measurement technique for long fiber thermoplastic material, SPE ACCE Proceedings, 2019.
12. C. W. Macosko, Rheology: Principles, measurements, and applications, Advances in inter-facial engineering series, New York, 1994.
13. T. A. Osswald, N. Rudolph, Polymer rheology: Fundamentals and applications, Hanser Publications, Cincinnati, 2015.
14. N. Meyer, Mesoscale simulation of the mold filling process of sheet molding compound, Doctoral thesis, Karlsruhe Institute of Technology (KIT), 2021.
15. E. S. G. Shaqfeh, G. H. Fredrickson, The hydrodynamic stress in a suspension of rods, Physics of Fluids A (1) (1990) 7–24.
16. K. Nakamura et al., Some aspects of nonisothermal crystallization of polymers. I. relationship between crystallization temperature, crystallinity, and cooling conditions, Journal of Applied Polymer Science 16 (1972) 1077–1091.

17. R. M. Patel and J. E. Spruiell: Crystallization kinetics during polymer processing—analysis of available approaches for process modeling, Polymer Engineering & Science 31 (1991) 730–738.
18. D. Kugele et al.: Henning, Modeling of the non-isothermal crystallization kinetics of polyamide 6 composites during thermoforming, AIP Conference Proceedings 1896 (2017) 030005.
19. J. D. Hoffman and J. J. Weeks: Rate of spherulitic crystallization with chain folds in polychlorotrifluoroethylene, The Journal of Chemical Physics 37 (1962) 1723–1741.
20. A. Ziabicki: Fundamentals of fibre formation: The science of fibre spinning and drawing, Wiley, London u.a., 1976.
21. J. M. Svanberg and A. J. Holmberg: Prediction of shape distortions Part I. FE-implementation of a path dependent constitutive model, Composites Part A: Applied Science and Manufacturing 35 (6), 2004.
22. G.P. Tandon and G. J. Weng: The effect of aspect ratio of inclusions on the elastic properties of unidirectionally aligned composites, Polym. Compos. 5 (4), S. 327–333, 1984
23. B. Rosen and Z. Hashin: Effective thermal expansion coefficients and specific heats of composite materials, International Journal of Engineering Science 8 (2), 1970.
24. W. Clayton: Constituent and composite thermal conductivities of phenolic-carbon and phenolic-graphite ablators, in: 12th Structures, Structural Dynamics and Materials Conference, American Institute of Aeronautics and Astronautics, Reston, Virigina, 04191971, 1971-380.
25. Sun et al.: Thermoplastic composite compression molding simulation, SPE-ACCE 2020 conference proceedings645, 2020.
26. Y. Chang et al.: Dynamic Property of the Frozen-Layer and its Effects on Warpage in Injection Molded Parts, Annual Technical Conference – ANTEC, Conference Proceedings, Chicago, IL, USA Vol. 5, pp. 2905, 2009.